PROCEEDINGS, 47th Workshop on Geothermal Reservoir Engineering
Stanford University, Stanford, California, February 7-9, 2022
SGP-TR-223

The EGS Collab – Initial Results from Experiment 2: Shear Stimulation at 1.25 km depth

Tim Kneafsey[1], Doug Blankenship[2], Pat Dobson[1], Jeff Burghardt[3], Mark White[3], Joseph P. Morris[4], Tim Johnson[3], Mathew Ingraham[2], Craig Ulrich[1], William Roggenthen[5], Thomas Doe[6], Megan Smith[4], Jonathan B. Ajo-Franklin[7], Lianjie Huang[8], Ghanashyam Neupane[9], Tatiana Pyatina[10], Paul C. Schwering[2], Chet Hopp[1], Veronica Rodriguez Tribaldos[1], Yves Guglielmi[1], Chris Strickland[3], Vince Vermuel[3], Pengcheng Fu[4], Hunter A. Knox[3], and The EGS Collab Team*

1. Lawrence Berkeley National Laboratory, Berkeley, California, USA
2. Sandia National Laboratories, Albuquerque, New Mexico, USA
3. Pacific Northwest National Laboratory, Richland, Washington, USA
4. Lawrence Livermore National Laboratory, Livermore, California, USA
5. South Dakota School of Mines & Technology, Rapid City, South Dakota, USA
6. Doe Geo, Redmond, Washington, USA
7. Rice University, Houston Texas
8. Los Alamos National Laboratory, Los Alamos, New Mexico, USA
9. Idaho National Laboratory, Idaho Falls, Idaho, USA
10. Brookhaven National Laboratory, Upton, New York, USA

tjkneafsey@lbl.gov

Keywords: Enhanced Geothermal Systems, EGS Collab, stimulation, crystalline rock, Sanford Underground Research Facility, coupled process modeling, experimental, field test, flow test

ABSTRACT

The EGS Collab project is performing intensively monitored rock stimulation and flow tests at the 10-m scale in an underground research laboratory to inform challenges in implementing enhanced geothermal systems (EGS). This project, supported by the US Department of Energy, is gathering data and observations from the field tests and comparing to understand processes and to build confidence in numerical modeling of the processes.

The now-completed Experiment 1 examined hydraulic fracturing in an underground test bed at the Sanford Underground Research Facility (SURF) in Lead, South Dakota, at a depth of approximately 1.5 km. We installed geophysical monitoring instrumentation in six of eight sub-horizontal boreholes in a well-characterized phyllite with many sensor types to allow careful monitoring of stimulation events and flow tests. The other two boreholes were also instrumented to perform and carefully measure water injection and production. We performed more than a dozen stimulations and nearly one year of flow tests in the testbed and collected and analyzed detailed observations

* J. Ajo-Franklin, T. Baumgartner, K. Beckers, D. Blankenship, A. Bonneville, L. Boyd, S. Brown, J.A. Burghardt, C. Chai, A. Chakravarty, T. Chen, Y. Chen, B. Chi, K. Condon, P.J. Cook, D. Crandall, P.F. Dobson, T. Doe, C.A. Doughty, D. Elsworth, J. Feldman, Z. Feng, A. Foris, L.P. Frash, Z. Frone, P. Fu, K. Gao, A. Ghassemi, Y. Guglielmi, B. Haimson, A. Hawkins, J. Heise, C. Hopp, M. Hom, R.N. Horne, J. Horner, M. Hu, H. Huang, L. Huang, K.J. Im, M. Ingraham. E. Jafarov. R.S. Jayne, T.C. Johnson, S.E. Johnson, B. Johnston. S. Karra, K. Kim, D.K. King, T. Kneafsey, H. Knox, J. Knox, D. Kumar, K. Kutun, M. Lee, D. Li, J. Li, K. Li, Z. Li, M. Maceira, P. Mackey, N. Makedonska, C.J. Marone, E. Mattson, M.W. McClure, J. McLennan, T. McLing, C. Medler, R.J. Mellors, E. Metcalfe, J. Miskimins, J. Moore, C.E. Morency, J.P. Morris, T. Myers, S. Nakagawa, G. Neupane, G. Newman, A. Nieto, T. Paronish, R. Pawar, P. Petrov, B. Pietzyk, R. Podgorney, Y. Polsky, J. Pope, S. Porse, J.C. Primo, T. Pyatina, C. Reimers, B.Q. Roberts, M. Robertson, V. Rodríguez-Tribaldos, W. Roggenthen, J. Rutqvist, D. Rynders, M. Schoenball, P. Schwering, V. Sesetty, C.S. Sherman, A. Singh, M.M. Smith, H. Sone, E.L. Sonnenthal, F.A. Soom, D.P. Sprinkle, S. Sprinkle, C.E. Strickland, J. Su, D. Templeton, J.N. Thomle, C. Ulrich, N. Uzunlar, A. Vachaparampil, C.A. Valladao, W. Vandermeer, G. Vandine, D. Vardiman, V.R. Vermeul, J.L. Wagoner, H.F. Wang, J. Weers, N. Welch, J. White, M.D. White, P. Winterfeld, T. Wood, S. Workman, H. Wu, Y.S. Wu, E.C. Yildirim, Y. Zhang, Y.Q. Zhang, Q. Zhou, M.D. Zoback

and numerous data sets of processes occurring during stimulation and dynamic flow tests. Data from these tests are generally openly available. Ambient temperature and chilled water flow tests were performed with many tracer tests to examine system behavior. We achieved adaptive control of the tests using close monitoring of rapidly disseminated data and near-real-time simulation. Numerical simulation was used to answer key experimental design questions, to forecast fracture propagation trajectories and extents, and to analyze and evaluate results. Many simulations were performed in near-real-time in conjunction with the field experiments, with more detailed simulations performed on a longer timeframe.

Experiment 2 is designed to examine hydraulic shearing in a new test bed at SURF at a depth of about 1.25 km in amphibolite under a different set of stress and fracture conditions than Experiment 1. A testbed is nearly complete consisting of 9 boreholes, in addition to two earlier-drilled characterization boreholes. Of the 9 boreholes, one is used for injection, four contain grouted instrumentation, and the remaining four are adaptively used for production and monitoring. The testbed construction optimized encounters with approximately five fracture set orientations. The testbed geology, hydrology, and geomechanical conditions are described, in addition to a description of the monitoring system, stimulation and flow system, and planned stimulations.

1 INTRODUCTION

Enhanced or engineered geothermal systems (EGS) offer tremendous potential as an energy resource supporting the energy security of the United States. Estimates exceed 500 GWe for the western US, surpassing the resource base hosted by conventional hydrothermal systems [*Williams et al.*, 2008]. EGS resource estimates for the entire United States range up to an order of magnitude larger [*Augustine*, 2016]. Implementing EGS will require (1) improving the understanding and efficacy of stimulation techniques under appropriate in-situ conditions allowing communication among multiple wells, (2) improving imaging and monitoring techniques for permeability enhancement and evolution, as well as associated microseismicity, (3) improving technologies for zonal isolation for multistage stimulations under elevated temperatures, (4) developing technologies to isolate zones for controlling fast flow paths and control early thermal breakthrough, and (5) developing scientifically-based long-term EGS reservoir sustainability and management techniques.

The EGS Collab project aims to refine our understanding of rock mass response to stimulation using accessible deep rock. We are performing 10 m spatial scale experiments under stress relevant to EGS. Our tests and analyses support validation of thermal-hydrological-mechanical-chemical (THMC) modeling approaches. We are also testing and improving conventional and novel field monitoring tools. We focus on understanding and predicting permeability enhancement and evolution in crystalline rock, including how to create sustained and distributed permeability for heat extraction from a reservoir by generating new fractures that complement existing fractures. The project has planned three multi-test experiments to increase understanding of 1) hydraulic fracturing (Experiment 1- field tests completed at the time of this writing), 2) shear stimulation (Experiment 2 – testbed construction underway), and 3) other stimulation methods in Experiment 3. Each series of tests within an experiment begins with modeling to support experiment design, and post-test modeling and analysis are performed to examine the effectiveness of our modeling and monitoring tools and approaches. By doing this, we can gain confidence in and improve the array of modeling and monitoring tools in use.

Experiment 1 was performed on the 4850 (foot depth, ~1.5 km) level at the Sanford Underground Research Facility (SURF, Figure 1) in Lead, South Dakota [*Heise*, 2015]. This experiment established a fracture network that connects an injection well and a production well using hydraulic fracturing [*Morris et al.*, 2018]. The test bed consisted of eight ~ 60 m continuously-cored subhorizontal boreholes. The boreholes were characterized using optical and acoustic televiewers, full waveform sonic, electrical resistivity, natural gamma, and temperature/conductivity logs [*Ulrich et al.*, 2018]. Six of the boreholes were monitoring wells that surrounded the experimental volume of rock. These boreholes contained grouted-in sensors [*Kneafsey et al.*, 2020]. Monitoring systems included electrical resistivity tomography [*Johnson et al.*, 2019; *Johnson et al.*, 2021], continuous active source seismic monitoring and passive seismic monitoring [*Ajo-Franklin et al.*, 2018; *Chai et al.*, 2020; *Chi et al.*, 2020; *Fu et al.*, 2021a; *Fu et al.*, 2019; *Pan et al.*, 2019; *Schoenball et al.*, 2019; *Schoenball et al.*, 2020a; *Schoenball et al.*, 2020b; *Schoenball et al.*, 2021; *Templeton et al.*, 2019], distributed temperature, strain, and acoustic monitoring [*Fu et al.*, 2021a]. The local stress regime is based on kISMET project characterizations [*Oldenburg et al.*, 2017; *Wang et al.*, 2017]. The injection and production boreholes were drilled into the experimental rock volume approximately parallel to the minimum principal stress direction. This was done so that hydraulic fractures would tend to propagate orthogonally to the injection well. More than a dozen stimulations were performed and the injection and production boreholes were connected [*White et al.*, 2019]. Flow tests were conducted using initially ambient temperature water and then chilled water (to model EGS) over the course of a year [*Kneafsey et al.*, 2021], and tracer tests were intermittently performed to understand flow conditions [*Mattson et al.*, 2019a; *Mattson et al.*, 2019b; *Neupane et al.*, 2020; *Wu et al.*, 2019].

All tests were analyzed before and after using a range of models, for example [*Fu et al.*, 2021a; *White et al.*, 2019; *White et al.*, 2021; *White et al.*, 2020; *White et al.*, 2018] in an attempt to better understand how to model the processes observed. Experiment 1 is well documented (e.g., *Dobson et al.* [2021]; *Kneafsey et al.* [2021]; *White et al.* [2019], Google Scholar, author "EGS Collab") and numerous available data sets (https://gdr.openei.org/egs_collab).

Experiment 2 is intended to investigate shear stimulation. The testbed for this experiment is being constructed on the 4100 (foot depth, ~1.25 km) level at SURF. The Experiment 2 testbed is in the Yates amphibolite and the subsurface stress conditions are different from those of Experiment 1 on the 4850 level [*Ingraham et al.*, 2020], and analyses have been performed in an attempt to understand shearing in this testbed [*Dobson et al.*, 2018; *Ingraham et al.*, 2020; *Meng et al.*, 2021a; *Meng et al.*, 2021b; *Singh et al.*, 2019]. Pre-test investigation of the 4100 level included mapping fractures and features that can be observed on the drift walls, and the drilling and logging of a 10 m horizontal borehole and a 50 m vertical borehole. The vertical borehole identified and penetrated a thick (~11 m) rhyolite layer. Eighteen stress tests have been performed in the vertical borehole (eight of these have used the Step-Rate Injection Method for Fracture In-Situ Properties (SIMFIP) tool [*Guglielmi et al.*, 2015; *Guglielmi et al.*, 2021a; *Guglielmi et al.*, 2021b; *Guglielmi et al.*, 2014]) to quantify

displacement during testing. These tests showed significant stress heterogeneity, with instantaneous shut-in pressures (ISIP - indicating minimum principal stress information) in the amphibolite below the rhyolite around 27.6 MPa (4000 psi), in the rhyolite around 18.6 MPa (2700 psi), and in the upper amphibolite around 21.4 MPa (3100 psi). Because of this stress heterogeneity, the Experiment 2 test bed is designed to be entirely *above* the rhyolite layer.

2 GEOLOGY

The general geology in the vicinity of Experiments 1 and 2 is dominated by an anticline that plunges to the southeast [*Lisenbee and Terry*, 2009]. The host rock in which Testbed 1 (on the 4850 level) was developed, on the west flank of the anticline, was entirely within a metasedimentary rock, a carbonate-mica phyllite of the upper Poorman Formation, whose characteristics are described more fully in *Caddey et al.* [1991]. Stratigraphically, this metasedimentary rock overlies an older amphibolite sequence called the Yates member of the Poorman Formation, which is the host rock for the new testbed on the 4100 level. The new testbed (Experiment 2) is located on the same anticline as Testbed 1 but it is nearer to the crest of the anticline (Figure 1). The Yates member consists of metamorphosed basalts and volcaniclastic sediments, forming a massive hornblende-plagioclase amphibolite schist, with lesser amounts of chlorite, quartz, and calcite [*Caddey et al.*, 1991; *Lisenbee and Terry*, 2009]. Several thin, sulfur-rich layers are exposed in the access drift near Testbed 2; these features are oxidized where visible but presumably contain unoxidized sulfides within the rock. These features represent geomechanically weak intervals and may reflect original bedding.

Although the host rock for the both experiments is of Precambrian age, a Paleogene (Tertiary) rhyolite occurs near and beneath the Testbed 2 volume. This rhyolite body is exposed in both the drift and in a reconnaissance borehole, TV4100 (drilled in 2019), which intersected a shallow-dipping rhyolite dike in a similar orientation to the exposures of rhyolite on the 4100 Level near the Yates shaft (Figure 1).

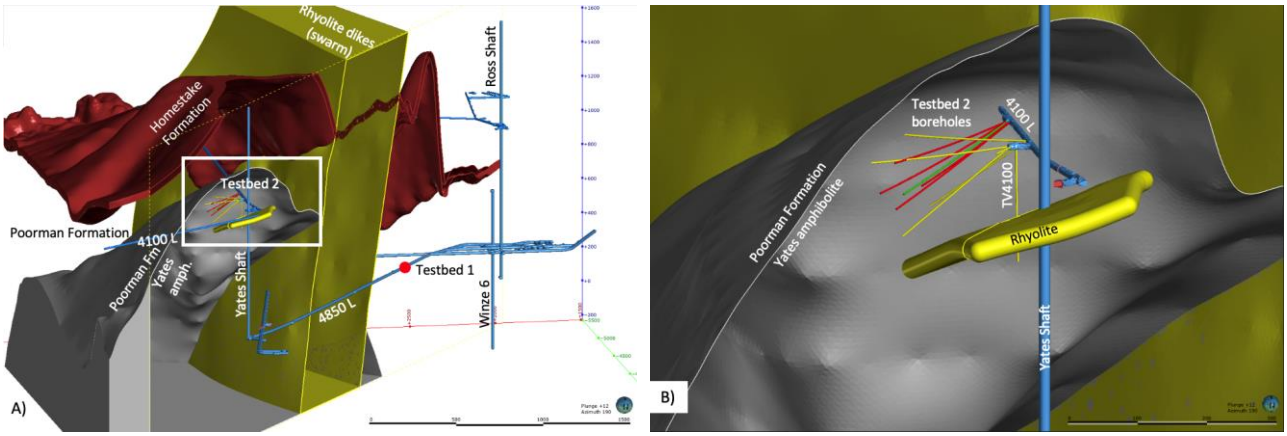

Figure 1. A. Representation of the geology of the rock hosting Testbeds 1 and 2. B. Enlarged region showing Testbed 2, the host rock, and location of the rhyolite. The monitoring wells are yellow, and test wells are red and green. The proposed injection well is green.

Detailed mapping of fractures was conducted in the drift and a nearby short intersecting alcove (battery alcove) to determine the nature and orientation of visible fractures. Three main classes of fractures were identified: foliation-parallel features, conjugate shear sets, and larger fractures interpreted to be Tertiary features associated with rhyolite dike emplacement. The photograph in Figure 2 shows the relation between the thin healed fractures of probable Precambrian age and a much larger Tertiary-age fracture. The higher angle fractures in Figure 2 possess infrequent small pore spaces of unknown connectivity, whereas the thin healed fractures do not provide such evidence.

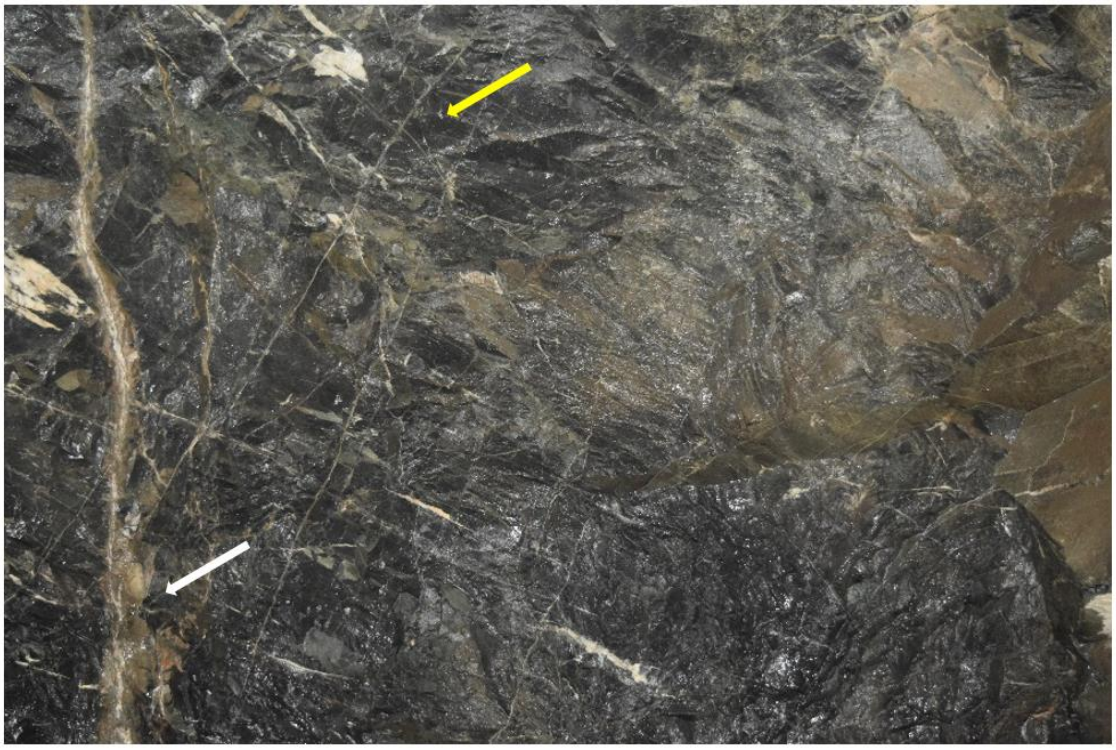

Figure 2. Fractures observed in the Battery Alcove on the 4100 level. White arrow points to large Tertiary fracture that can be traced over 5 m within the alcove and drift; yellow arrow indicates an example of a conjugate shear set.

2.1 Core examination

Continuous core samples were collected from each of nine testbed boreholes. The cores were logged and described during drilling operations, with selected intervals re-examined at the surface. Comparison of core from Testbed 1 and Testbed 2 showed significant differences in the rock fabric (Figure 3) due to the different modes of formation; i.e., layered sedimentary deposits as opposed to an igneous origin for the amphibolite.

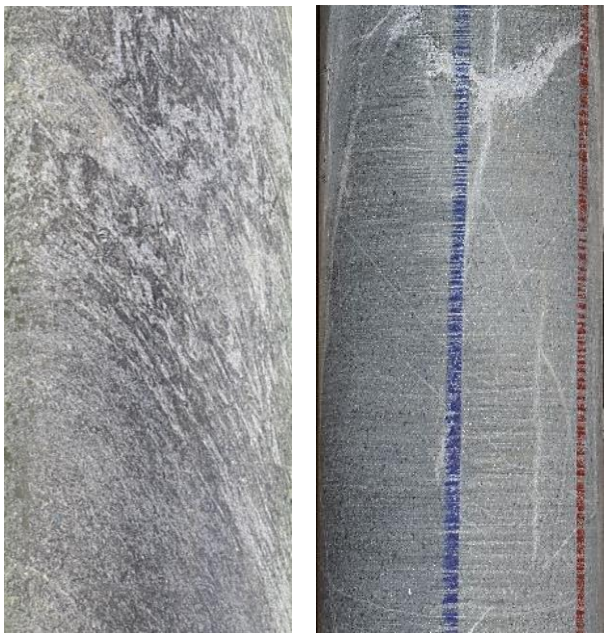

Figure 3. Example of core from Experiment Test Bed 1 (Experiment 1 left) and Test Bed 2 (Experiment 2 right). The carbonate mica phyllite in Experiment 1 shows prominent layering whereas the amphibolite from Experiment 2 is massive with many healed fractures.

In the case of Experiment 2, the results of the core examination were consistent with the observations made in the drifts (Figure 2). The vast majority of the fractures observed in the core were healed and filled with quartz, calcite, and minor sulfides. Small vugs (<0.5 mm) were observed infrequently, and testing with a hand-held permeameter yielded only limited connectivity. However, in several intervals the amphibolite was heavily altered, presumably by the intrusion of nearby rhyolite. The altered amphibolite is a greenish-gray color with numerous small (healed) fractures; in two notable instances, large open fractures have been preserved (Figure 4). The degree of shearing associated with the alteration varies from none to at least one instance where the central portion of this zone exhibits a plastic (clay-like) behavior.

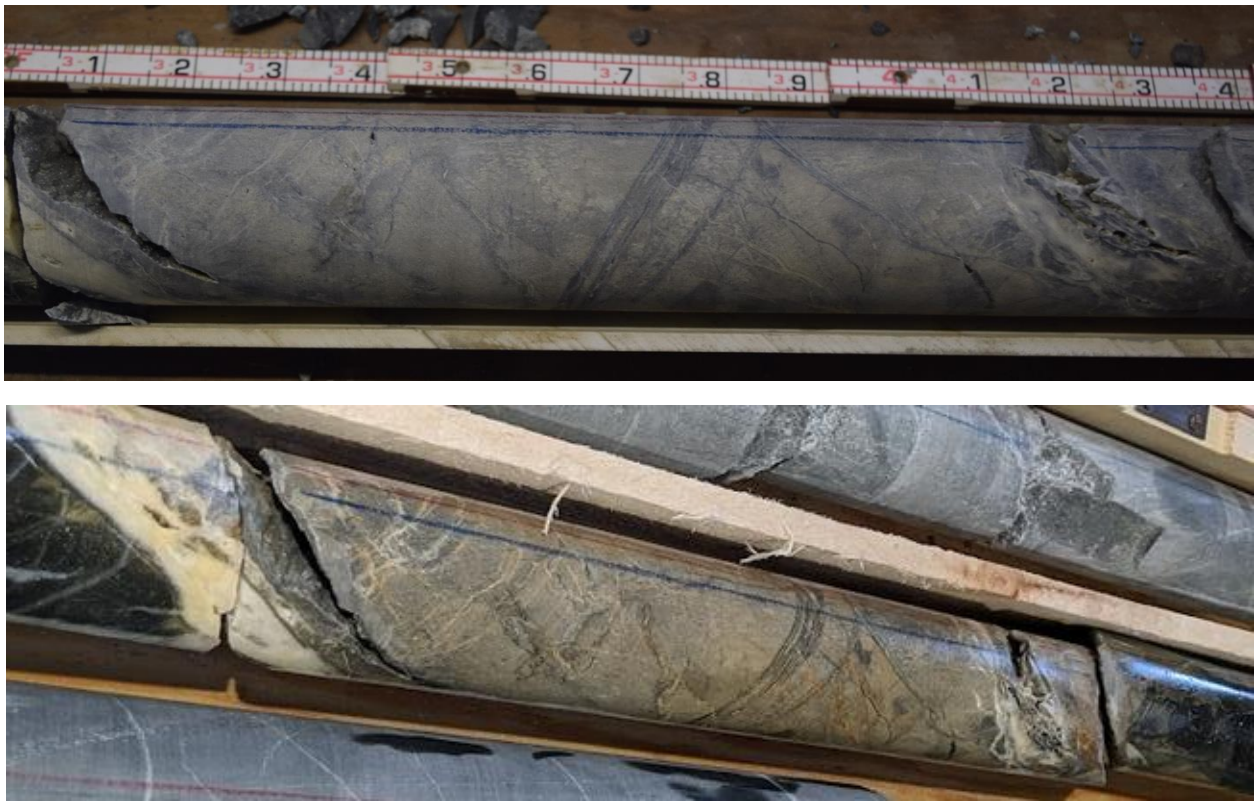

Figure. 4. Core photo of E2-AML at ~187 feet deep, showing some open portions of a highly fractured interval.

More detailed fracture analysis is being conducted on optical and acoustic televiewer logs collected from all of the new testbed boreholes described below. These new data will be used to identify appropriate intervals within the main injection borehole (E2-TC) to attempt hydraulic shear stimulation (the focus of Experiment 2).

3 EXPERIMENT 2 DESIGN

One of the first design considerations for Experiment 2 was the reduced space available on the 4100 level drifts. For Experiment 1, we were able to utilize a wide, double-track portion of a drift on the 4850 level for the entire length of the testbed. This allowed us to avoid any additional excavation to accommodate drilling, stimulation, flow, and monitoring equipment. Figure 5 shows schematically two of the options that were considered for utilizing space on the 4100 level. Early in the design process, there was concern that budget would only allow limited excavation. Consequently, a concept was developed that would utilize a limited stretch of double track in combination with a preexisting battery alcove (Figure 5, left). While reducing the cost, this approach would have multiple disadvantages, including limited space margins in the battery alcove and the necessity that significant tubing and cabling be run down the drift between the double-track and the battery alcove. Ultimately, sufficient budget was secured to support several excavations to extend the battery alcove and construct two additional alcove areas to accommodate stimulation and monitoring equipment (Figure 5, right).

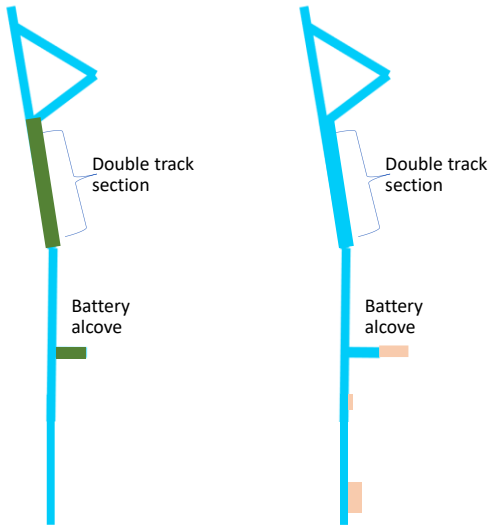

Figure 5: Space was a major consideration for experimental design on the 4100 level. Plans were developed in the event of no budget for additional excavation (left) and significant excavation (right). Ultimately, the project was able to support a design similar to that on the right. Green areas correspond to preexisting portions of the drift complex. The peach areas indicate potential excavations.

The orientations of the injection and production wells were selected to increase the likelihood of intersecting natural fractures that are favorably oriented for shear reactivation. The analysis considered five fracture set orientations (see **Error! Not a valid bookmark self-reference.**) identified from the drift wall and borehole observations. We developed a model of the stress field based upon observations from the characterization wells and estimated a minimum horizontal stress of 18.3 MPa with an azimuth of 24 degrees, dipping 28 degrees from the horizontal. The maximum horizontal stress, vertical stress and pore pressure were estimated to be 37.3 MPa, 36 MPa, and 4.23 MPa, respectively. Figure 6 shows the estimated slip tendency for the five joint sets under this assumed stress state. We observe that sets 1, 4, and 5 are oriented most favorably for shear activation. During the design phase, the specific locations of fractures were not known as drilling had not been completed. Because of that, it was decided to have multiple production wells (E2-TL, E2-TU, E2-TN, E2-TS, where "T" stands for "test". "L" for lower, "U" for upper, "N" for north, and "S" for south) surrounding the injection well (E2-TC, "C" for center), (Figure 7). In this manner, it can be expected that stimulated fractures will intersect at least one production well. Schematics of the Experiment 2 well layout are shown in Figures 1 and 7. In this testbed, we envisioned our injection borehole (green) and production borehole(s) (red) to fan out providing different distances between the wells depending on the depth from the collar. Monitoring wells (E2-DMU, E2-DML, E2-AMU, E2-AML, where "D" stands for drift, "M" for monitoring, "A" for alcove) are oriented to span the volume of interest on as many sides as possible at a larger distance than was used in Experiment 1. Consequently, we have two pairs of monitoring wells oriented approximately orthogonal to the injection well above and below the stimulation zone. One monitoring well, however, is oriented subparallel to the stimulation well. Geophysical sensors used and their deployment in Experiment 2 have been redesigned based on learnings from Experiment 1, although the range of sensors used will be similar to those deployed in Experiment 1. The new sensors are more robust (e.g., tubing encapsulated cable), and the sensor layout in the monitoring wells is different. A large diameter PVC shroud is centralized in the well having the ERT electrodes and fiber on the outside, and the seismic sources and receivers inside (See Monitoring System Design). The disks in Figure 7 indicate potential natural fractures that connect the injection and projection wells, and hotter colors indicate greater slip tendency. Equal numbers of fractures within each joint set were randomly placed within the stimulated volume and we only show fractures that intersect the injection and production wells. Figure 7 indicates that this design is expected to intersect mostly fractures within JS1, which we have estimated to have high slip tendency (Figure 6). Analyses were performed using the Fat Crayon Toolkit [*Morris*, 2021].

Table 1: Five fracture set orientations were identified and were considered during design of Experiment 2.

Name	Strike	Dip
JS1	155.0	55.0
JS2	20.0	27.0
JS3	280.0	50.0
JS4	265.0	70.0
Sulfide layer (JS5)	50.0	40.0

Extensive simulations of hydraulic stimulations were performed during the Experiment 2 design phase. In addition to shear stimulation, we also consider hydraulic fracturing. This is because the outcome of hydraulic shearing depends highly on in situ characteristics of natural fractures known to be highly variable and difficult to measure. Because the uncertainties in the simulation parameters are greater than the value of hydraulic shearing simulations in the design phase, we focused on two simulation tasks that can directly impact testbed design decisions:

1. Predict the propagation trajectory of a potential opening-mode hydraulic fracture.

2. Predict the breakdown pressure in the near-wellbore region for identified natural fractures.

Detailed results on the first simulation task are reported in *Fu et al.* [2021b]. Results on the second task are being reviewed.

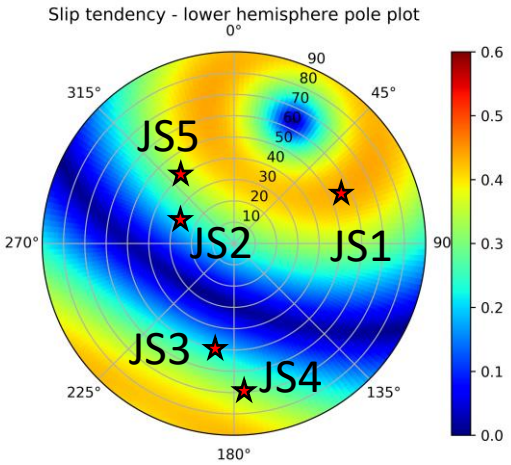

Figure 6: Slip tendency plot for the five identified joint sets. The slip tendency is the coefficient of friction required to avoid slip under the assumed stress conditions. Consequently, higher slip tendency indicates an orientation closer to slip. For the assumed stress state, sets 1, 4, and 5 are oriented most favorably for slip.

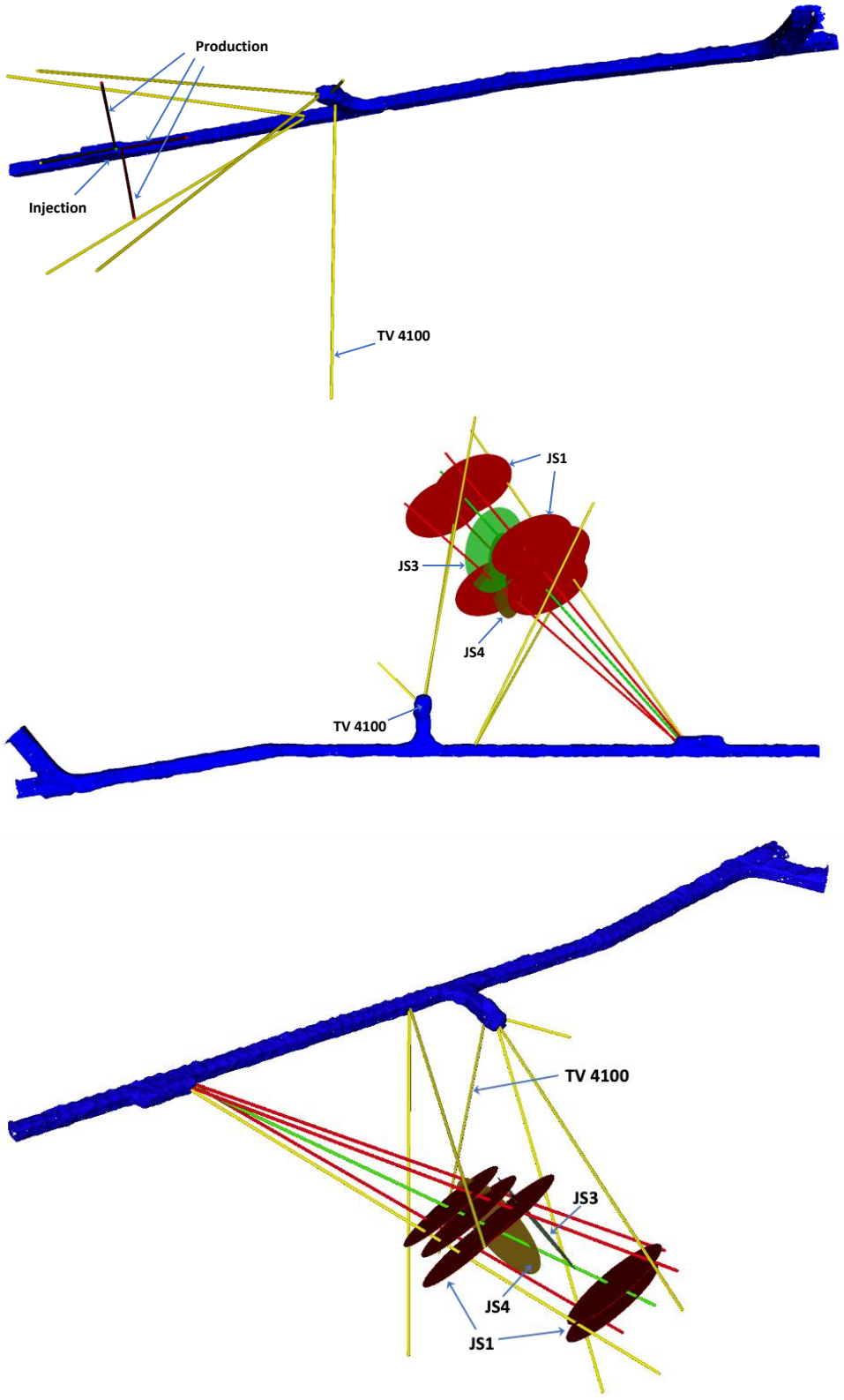

Figure 7. Well orientations for Experiment 2, shown from different perspectives (top – from above; center – oblique from below; bottom – oblique from the side). The thick blue object represents the drift, the green line represents the injection well, red lines represent production wells, and yellow lines represent monitoring wells. Other than the vertical well TV4100, all wells are subhorizontal. Disks indicate potential natural fractures that connect the injection and projection wells and hotter colors indicate greater slip tendency. We observe that this design is expected to connect fractures within JS1 which have high slip tendency.

4 TESTBED CHARACTERIZATION

4.1 Wireline Characterization

A suite of geophysical wireline tools was used to characterize the rock and fractures within the Experiment 2 testbed. Understanding the thermal gradient away from the drift is important, as are the changes in rock types within the testbed, fracture types (including healed, open, flowing), rock foliation, formation fluid conductivity, rock resistivity and acoustic velocities, and the final borehole orientations. To collect this information, we used a *Mt. Sopris* logging system that coupled a *Matrix* data logging unit to a series of downhole geophysical probes: Fluid Temperature and Conductivity, Optical and Acoustic Borehole Imaging, Electrical Resistivity, Full Waveform Sonic, and a North-seeking gyro by Axis Mining Technology. Logs from these tools were run in all 9 boreholes in the Experiment 2 testbed, along with the TV4100 characterization borehole, resulting in 56 high resolution log data sets. Temperatures near the drift in well TC (likely stimulation well) started around 25°C and increased to around 30°C at the end of the borehole, 80 m from the drift. This gradient is not as steep as the gradient observed in the Experiment 1 testbed, consistent with lower background rock temperatures expected at the shallower drift depth. Rock resistivities ranged from 100 – 100k Ohm-m. Natural gamma spikes at changes in rock types and/or at fractures with fine fault-gouge sediments were observed along with associated resistivity decreases (Figure 8). Gamma spikes are generally associated with increases in clay content and/or potassium-bearing rocks or fractures. Rock acoustic velocities in the near-wellbore were investigated with a three-receiver unit. P-wave velocities ranged from 5,000 – 8,000 m/s and shear wave velocities ranged from approximately 2,500 – 4,000 m/s. The optical and acoustic borehole imagers captured numerous fractures throughout the length of each borehole, resulting in approximately 1300 fractures (healed and open fractures, filled veins, etc.) that were picked to identify fracture sets with specific orientations which would be used in a slip tendency analysis to select favorable fractures for later stimulations. These fractures can also be used to develop a discrete fracture network model. An example of some picked fractures is shown in Figure 9.

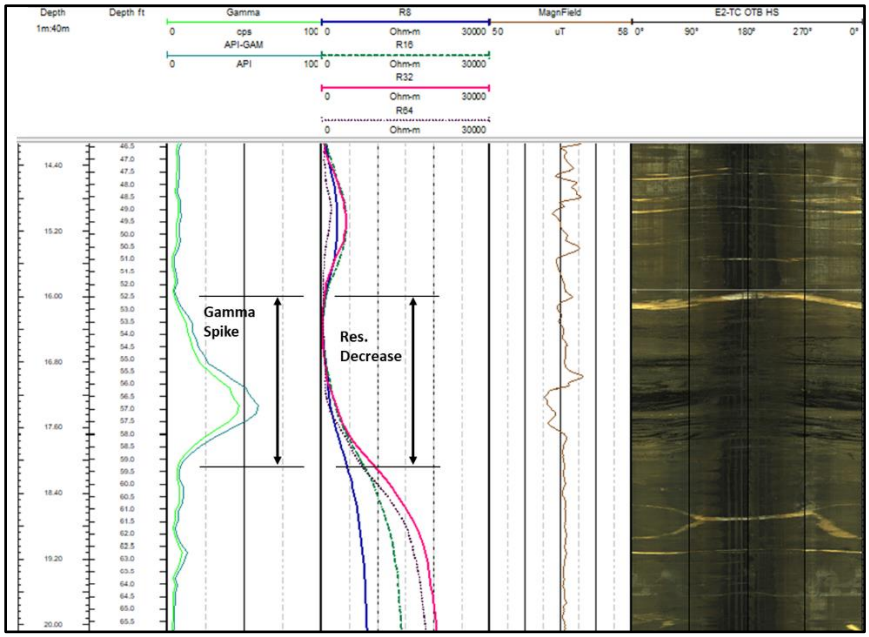

Figure 8: Resistivity – Gamma log with Optical Borehole Imager that shows a gamma spike associated with a change in rock type and a resulting decrease in resistivity (Borehole E2-TC – planned injection well).

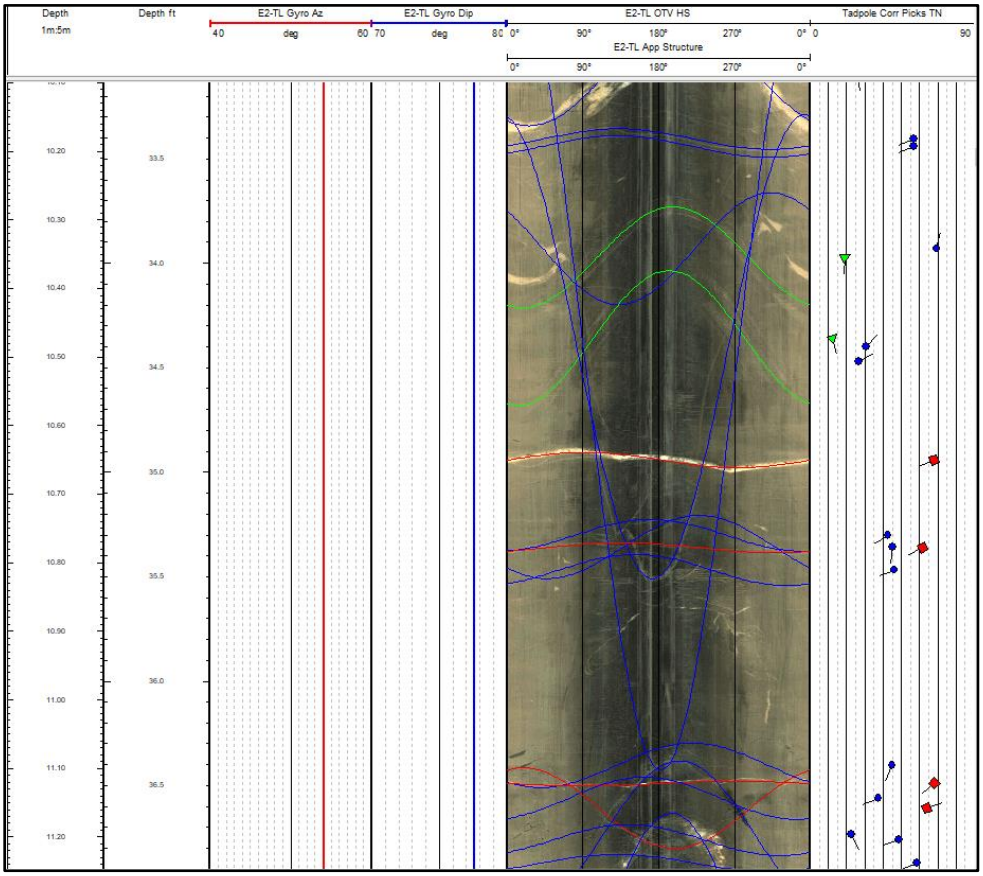

Figure 9: Optical Borehole Imager log showing different types of features (green – foliation, blue – healed fractures/veins, and red – open fractures) (Borehole E2-TL, beneath the planned injection well).

4.2 Hydraulic Characterization

4.2.1 Observations and ambient pressure measurements

The testbed is located 4100 ft (1250 m) below ground surface (bgs) with the nominal water table located at 80.7 m below the ground surface, yielding a potential hydrostatic pore pressure of 11.47 MPa. Earlier mining operations, prior to closure of the Homestake Mine in 2002, included active water pumping to 8,000 ft (2,438 m) bgs (the current water level at SURF is ~5700 ft bgs). The testbed is located laterally near the vertical Yates shaft (Figure1), which was started in 1938 and extends to about 5000 ft, making the testbed within the drained region. The current pore pressure in the region of the test bed is heterogenous. The hydrostatic head to the shallow water table provides an upper limit to the pore pressure at the 4100 level of about 12 MPa; however, pore pressure measurements in boreholes drilled for the DUSEL experiment at the 4850 level [*Stetler*, 2015] showed that most were non-flowing and the three that did flow yielded pore pressures that were between 15% and 60% of hydrostatic.

In the Experiment 2 test bed area there are flowing fractures along the drift in rhyolite ~100 m from the test bed near the Poorman-Yates formation contact. A vertical exploration hole for our Experiment 2 produced <0.1 liter/min water from a fracture in a rhyolite dike at a pressure measured as high as 200 psi (1.4 MPa or ~11% of hydrostatic). Of the Experiment 2 boreholes only one produced water with a rate of ~ 0.2 l/min, without a pressure measurement.

Other than the one flowing zone, careful monitoring of the inflows and outflows of the Experiment 2 boreholes during drilling showed:

- No evidence of connected fractures based on circulation during drilling (such fractures had been observed in Test Bed 1 at the 4850 level) and
- All flows were water losses *to* the rock with the exception of E2-DMU and some initial outflows from E2-AML before it began losing water.

The water loss data in Figure 10 show the cumulative losses over the drilling period give flow rates that range from approximately 20-180 ml/day. The water losses indicate flow to a sink at a lower elevation than the experiment, and a likely candidate for the that sink would be the nearby Yates Shaft. While the presence of flowing fractures in the vicinity of the test bed indicates highly heterogeneous fracture connectivity and pore pressure distributions, we expect the mine drainage is the main influence on pore pressures, and the pore pressure value will be a relatively small, if not negligible fraction of the pressures required to open or stimulate fractures in the test bed.

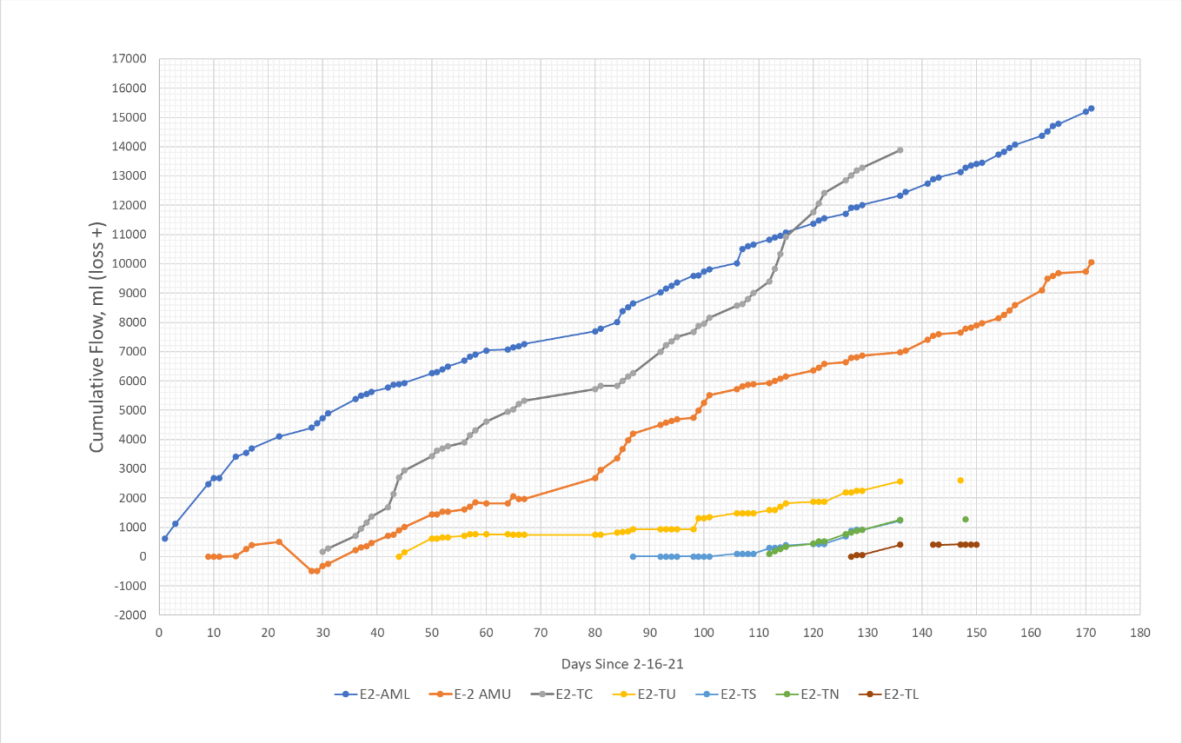

Figure 10. Water balance tracking on monitoring and test boreholes of Experiment 2.

4.2.2 Packer Hydraulic Characterization Tests

A major target of Experiment 2 is shear stimulation of a naturally conducting fracture. With only a few exceptions the fractures in the Experiment 2 test bed are healed and show little indication of being significantly transmissive. The water losses show the rock has some conductivity, and packer tests were performed to try to locate sections of preferential fracture transmissivity. The tests used a single low-pressure packer to determine hydraulic conductivity using pressure pulse tests, which look at pressure decay after charging a test zone with a pressure pulse. The volume of flow into the test section can be determined from the pressure decay and the total compressibility of the test zone and the test equipment.

For these tests we used the mine water as pressure-pulse source (~0.5 MPa). Given the low conductivity of the rock, the pressure pulses decayed by only about 10% over the 30-minute test durations. The 30-minute pulse decay was followed by a 2-3 minute constant-rate injection to obtain the total compressibility for calculating the water loss to the borehole during the pulse decay period (Figure 11). Dividing this loss by the time-duration of the pulse gives a flow rate for calculation of transmissivity and hydraulic conductivity assuming steady state flow. The pressure pulse tests were performed over the entire open length of each borehole, except borehole E1-TC. In the E1-TC borehole, the planned stimulation-source borehole, the hydraulic characterization tests were conducted with the single packer located at four depths (i.e., 30, 100, 150, and 200 ft (9.1, 30.5, 45.7, and 61.0 m.) to try to isolate transmissive candidate fractures for stimulation.

The pressure-pulse results (Table 2) show that the rock has a uniformly low permeability with total-borehole values ranging from 6.9×10^{-19} to 4.6×10^{-18} m^2 for the majority of the tests. The values for the borehole with the flowing zone, E2-DMU, are based on its measured flow of 180 ml/min and an assumed head of 1.4 MPa based on the measured pressure value in TV4100. The results of the four tests in E2-TC suggest that the bottom portion of the borehole (below 200 ft or 61 m) may be slightly more transmissive than the rest of the borehole.

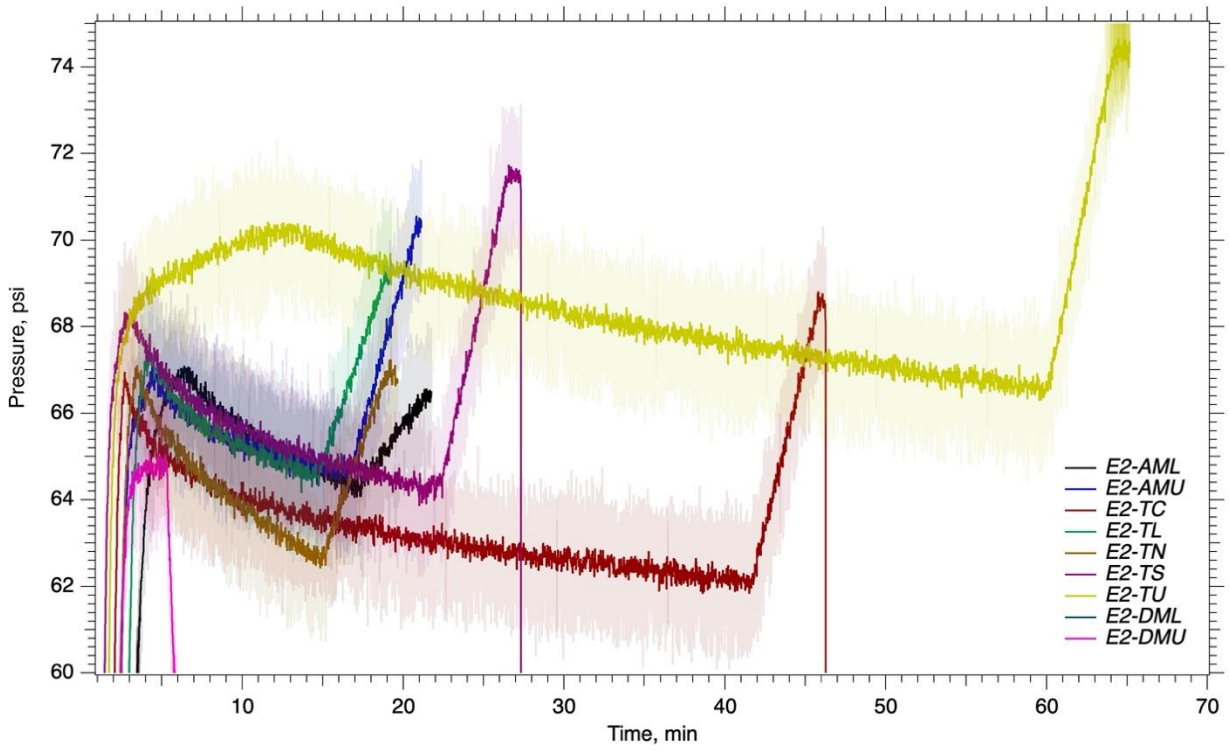

Figure 11. Pressure response of monitoring and test boreholes during hydraulic characterization test for Experiment 2.

Table 2. Hydraulic test results.

Borehole	Packer Set Depth (m)	Zone Length (m)	Transmissivity (m^2/s)	Hydraulic Conductivity (m/s)	Permeability (m^2)	Test Type
E2-TC	9.1	68.0	1.8E-09	2.7E-11	2.7E-18	Pressure-Pulse
E2-TU	9.1	67.4	4.7E-10	6.9E-12	6.9E-19	Pressure-Pulse
E2-TL	9.1	67.4	2.0E-09	2.9E-11	2.9E-18	Pressure-Pulse
E2-TN	9.1	67.4	3.1E-09	4.6E-11	4.6E-18	Pressure-Pulse
E2-TS	9.1	71.9	1.5E-09	2.1E-11	2.1E-18	Pressure-Pulse
E2-DML	9.1	46.0	1.5E-09	3.3E-11	3.3E-18	Pressure-Pulse
E2-DMU	9.1	45.7	2.2E-08	4.8E-10	4.8E-17	Steady Outflow
E2-AML	9.1	51.2	4.0E-09	7.9E-11	7.9E-18	Pressure-Pulse
E2-AMU	9.1	51.2	1.3E-09	2.5E-11	2.5E-18	Pressure-Pulse
E2-TC	30.5	46.6	1.5E-09	3.3E-11	3.3E-18	Pressure-Pulse
E2-TC	45.7	31.4	2.0E-09	6.5E-11	6.5E-18	Pressure-Pulse
E2-TC	61.0	16.2	2.2E-09	1.3E-10	1.3E-17	Pressure-Pulse

5 MONITORING SYSTEM

5.1 Design

The geophysical monitoring system consists of a comprehensive suite of downhole sensing instrumentation including active seismic, passive seismic, fiber-based distributed temperature (DTS), strain (DSS), and acoustics (DAS), and electrical resistivity tomography (ERT), designed to provide autonomous and concurrent multi-parameter sensing during flow and stimulation operations. The sensor layout is shown in Figure 12. Downhole sensing components in the yellow boreholes aligned approximately orthogonal to the injection well will be grouted in place using the grout design discussed below. The remaining (blue and gray) monitoring boreholes will be left ungrouted to

enable geophysical monitoring instrumentation to be removed and replaced with flow testing instrumentation (e.g., packer systems and associated sensors) as needed to optimize testing objectives. Each open borehole was water-filled to maintain energy coupling (e.g., seismic, electrical and thermal) with the formation during characterization and monitoring.

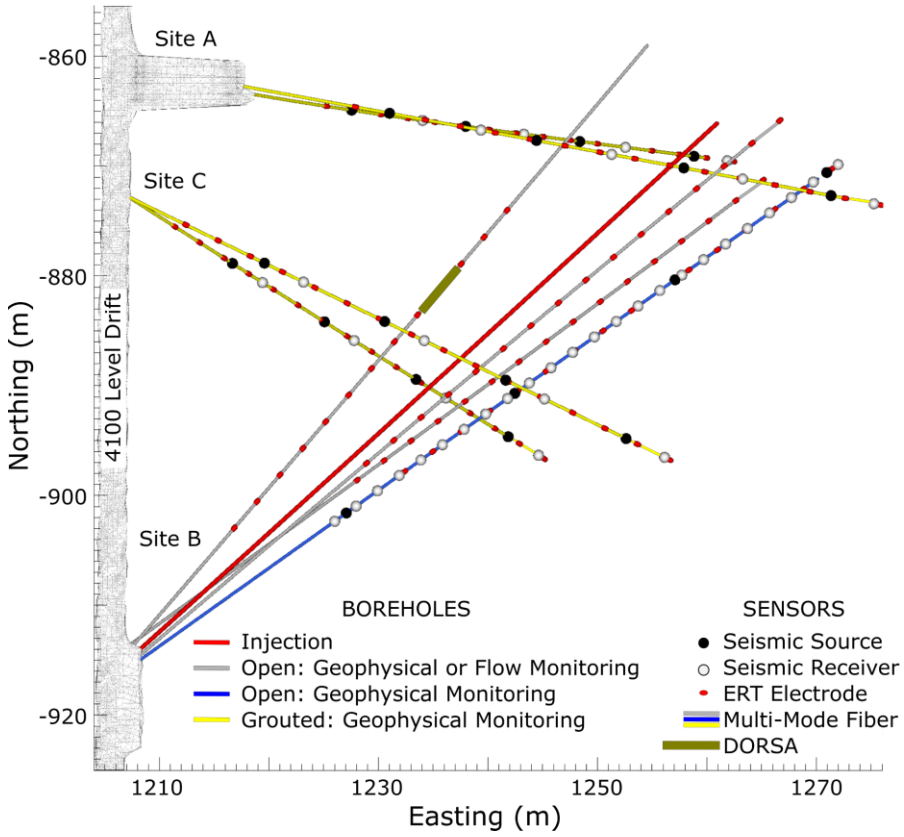

Figure 12. Plan view of geophysical monitoring borehole layout and sensor locations.

The instrumentation strings in each monitoring borehole were designed to reduce crosstalk between the seismic and ERT monitoring components, thereby enabling both to operate simultaneously. First, ERT electrodes and DTS/DAS/DSS fiber were attached to a 2.5 in PVC shroud and advanced downhole as shown in Figure 13 (left). Second, a wellhead designed to seal the annulus during grouting was installed. Third, the seismic instrumentation string was installed on inside of the PVC shroud as shown in Figure 13 (right). Finally, grout will be pumped into the grout inlet (Figure 13) to flow and fill the annulus between the PVC shroud and borehole wall. The shroud was left open at the bottom of the borehole, which enables a grout return pathway through the inside of the PVC shroud to seal the seismic instrumentation in place.

In comparison to the Experiment 1 design, many components were also hardened for increase durability during high pressure fracturing operations. Fiber optic components were deployed in very thin 316 SS tubes (2.2 mm) coated in HDPE to prevent interference with ERT measurements. Seismic sensors (3C accelerometers) and sources (piezoelectric transducers) were also deployed on tubing encapsulated conductors (TEC: 4 mm, 316 SS) to prevent damage. Component seals were selected with ratings to at least 5000 psi.

Beyond rugged packaging, one key design improvement was inclusion of a higher frequency 3-component (3C) accelerometer package for microseismic monitoring. The selected 3C sensor (MMF, KS943B100) is +- 3 dB to 22 kHz, providing a flatter response to accurately capture the spectrum of small events. The unusual shape of this sensor (flat diamond) also necessitated the development of a custom 316 SS sensor pod, visible within the PVC shroud in Figure 13 (right). In total, 16 3C accelerometers are included in the microseismic array, fully bracketing the planned stimulation zone. In addition to the accelerometer array, a dense array of 24 hydrophones will be deployed in one of the central wells to improve tomographic imaging coverage in the active source portion of the experiment.

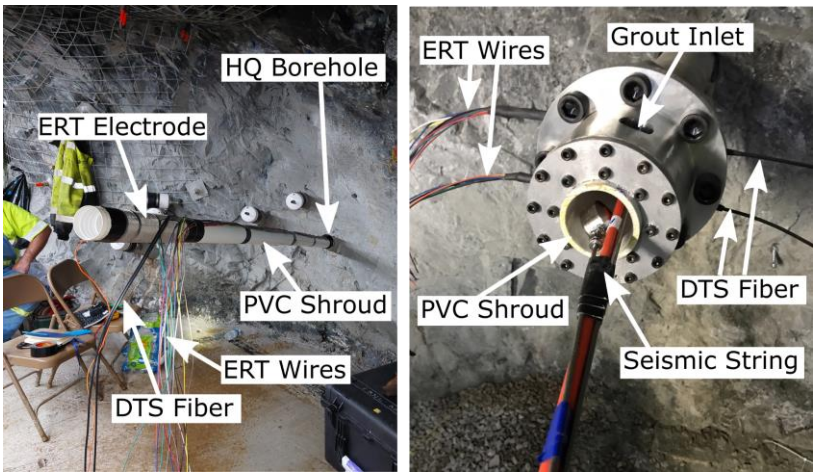

Figure 13. (left) Installation of ERT electrodes and DTS fiber on outside of monitoring well shroud. (Right) Installation of seismic instrument string on inside of monitoring well shroud.

As mentioned before, the microseismic monitoring component of the experiment will use the 3C accelerometers in the four grouted monitoring wells, visible as green lines in Figure 14 surrounding the stimulation region with four accelerometers in each well, centered at the stimulation region. Before deployment, we performed numerical modeling of microseismic hypocenter inversion performance to determine the optimal accelerometer separation. We obtain the relationships between the standard deviation error and the accelerometer interval for monitoring microseismic events around the stimulation region and those distributed in a region orthogonal to the stimulation well, as shown in Figure 14. We added Gaussian noise to synthetic travel time picks for event location analyses, to account for errors in the velocity models and travel time picks. Our numerical modeling suggested that the optimal receiver interval for the four geophones in each well is around 30-40 ft (~9.1-12.2 m), an estimate which guided the installation. The spacing of the ERT electrodes was also optimized in the design phase.

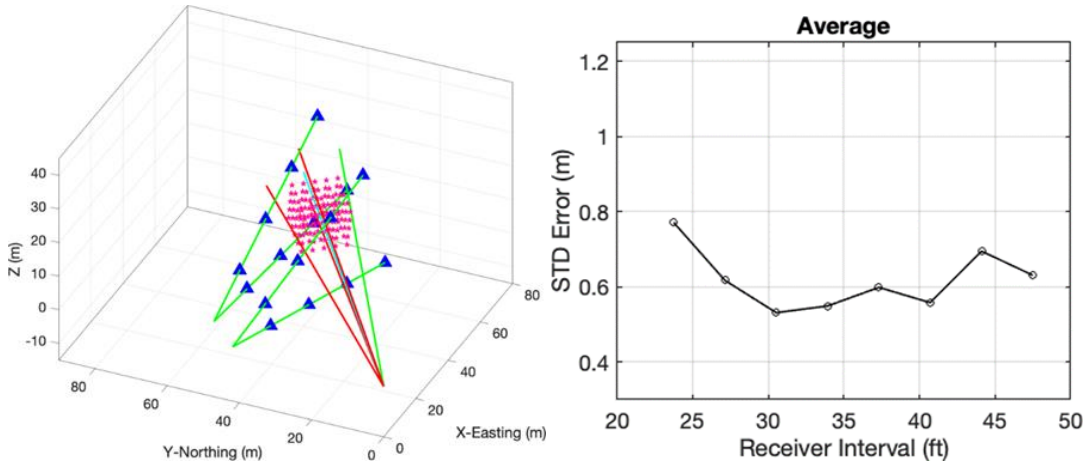

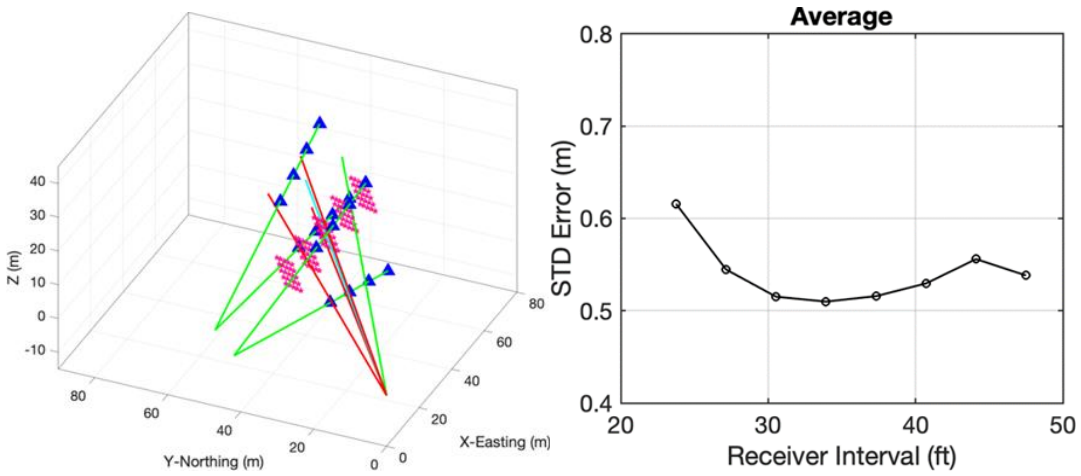

Figure 14: Top left panel: monitoring microseismic events (red stars) around the fracture stimulation region. Top right panel: The standard deviation error of microseismic event locations for the events in the top left panel vs. the receiver interval when using four accelerometers in each well, showing that the optimal receiver interval is around 30-40 ft. Bottom left panel: monitoring microseismic events (red stars) distributed in regions orthogonal to the stimulation well. Bottom right panel: The standard deviation error of microseismic event locations in the bottom left panel vs the receiver interval when using four accelerometers in each well, showing that the optimal receiver interval is also around 30-40 ft.

The downhole robotic strain analyzer (DORSA) and SIMFIP [*Guglielmi et al.*, 2015] tools will be used in Experiment 2. They are borehole-based tools that measure strain in 3 dimensions across a fracture or fault. Both consist of a sensing element having six tendons in which strain is measured. Either side of the sensing element is stabilized against the nearby rock. Although there are many differences, for their use here the SIMFIP is placed between high pressure packers allowing measurement while stimulating under high-pressure. In its current embodiment, the DORSA is not a high-pressure tool, but suitable for use in low-pressure monitoring wells.

5.2 Grout design for monitoring wells

To preempt difficulties experienced in Experiment 1 with grouted boreholes, a new grout mixture was designed and tested. The grout used to secure the suite of instruments in the monitoring holes and to seal them preventing the movement of fluids along the length of the wells was designed to have electrical resistivity of approximately 1000 Ohm-m, the heat of hydration temperature not exceeding the temperatures allowed by the installed instruments and their cables insulation (<80°C), and rheological parameters to easily flow into tight spaces between the cables and the equipment while still being stable and able to provide a tight seal against the cable insulation and a PVC pipe (no shrinkage) (for details see paper of Sollohub et al. "High Resistivity Well Cement for Underground Wells Suitable for Sealing Monitoring Equipment" this workshop). Grouting the boreholes will begin soon after the submission of this paper.

6 STIMULATION PLAN

6.1 State of Stress

As mentioned, one principal objective of Experiment 2 is to shear stimulate a natural fracture within the testbed, creating a hydraulic connection between two test boreholes. Shear stimulation requires a natural fracture or plane of geologic discontinuity with moderate permeability oriented such that it is under a shearing stress state. Shearing of the fracture surfaces occurs when fluid pressure within the fracture reduces the normal stress sufficiently for the shear forces to overcome cohesive forces. The stress state within the testbed is currently uncertain, but two hypotheses have been developed to explain the non-vertical orientations of induced fractures generated from stress measurements made in the vertical monitoring borehole TV4100 [*Burghardt et al.*, 2020]. The first hypothesis is that the minimum principal stress is dipped from horizontal, and the second is that there is a persistent plane of weakness, such as a natural fracture set, that yields induced fractures in that orientation. A Bayesian Markov Chain Monte Carlo uncertainty quantification analysis was completed to compute probability distributions for the principal stress magnitudes and orientations, based on elasticity solutions for the stress surrounding a vertical borehole with arbitrary principal stress magnitudes and directions. This analysis shows higher probabilities for tilted principal stress orientations (i.e., the principal vertical stress is not aligned with the gravitational direction). The stress orientation and magnitudes provide information about the shear stresses on natural fractures identified in the test boreholes. Fracture permeability data (Table 2) are also needed to identify a natural fracture as having slip potential. Detailed core and borehole televiewer observations were also made to identify prospective fractures that may connect the injection borehole (E2-TC) with one or more of the surrounding production boreholes. Another complicating feature is that almost all of the fractures are mineralized, which might make shear stimulation of such features more challenging (e.g., *Meng et al.* [2021a]).

6.2 Stimulation Design

Because few fractures with significant permeability were identified, the planned stimulation protocol focuses on fractures with the highest shear-to-normal stress. Figure 15 shows lower hemisphere pole plots of the fractures in E1-TC identified with each fracture being colored according to the expected value of the shear to mean stress ratio for these two stress state hypotheses. As the figure shows, the shear-to-

normal stress ratio is relatively low, with the highest values being approximately 0.25 and 0.35 for the two stress hypotheses. This is in contrast to a nominally expected critical friction coefficient of 0.6, which means that even in the absence of significant cohesion no fractures are expected to be close to incipient shear failure.

The planned stimulations will select a few of the fractures with the highest shear-to-normal stress for each stress state hypotheses to target. Each targeted fracture will be isolated with a straddle packer assembly and the subjected to 500 psi (3.5 MPa) until the flow rate reaches steady state. This step is to characterize the initial hydraulic properties of the fracture in a more detailed way than the prior lower pressure hydraulic characterization tests. Next, the zone will be pressurized to 2200 psi (15.2 MPa), which is approximately 83% of the minimum expected value of the minimum principal stress and only 30% of the well pressure that is estimated to be required to generate a tensile stress at the borehole wall. This pressure is therefore very unlikely to initiate a tensile hydraulic fracture. Any increase in permeability of the zone will therefore be a strong indication of shear stimulation. Measurements using the SIMFIP tool [*Guglielmi et al.*, 2014] will also quantify shear displacement. Because of the expected low permeability of the targeted natural fractures, a significant amount of time may be required to allow the applied pressure to diffuse into the natural fracture and initiate shear slip. It is planned to hold several of the fractures under pressure for at least overnight to several days to provide the best possible chance of shear stimulation.

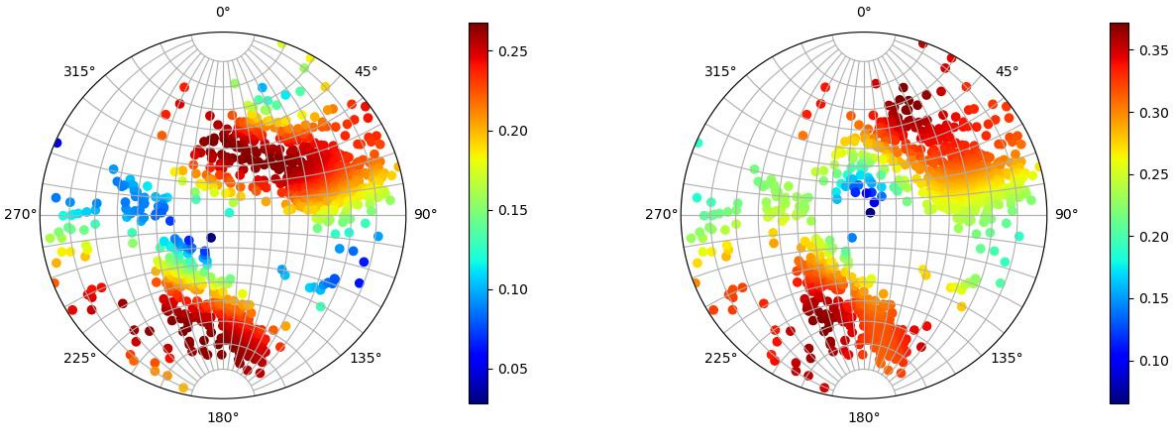

Figure 15. Left - Equal angle lower hemisphere projection of poles of identified fractures in E2-TC, colored according to the mean shear-to-normal stress ratio under the hypothesis that the principal stresses are rotated from vertical/horizontal. Right - Equal angle lower hemisphere projection of poles of identified fractures in E2-TC, colored according to the mean shear-to-normal stress ratio under the assumption that the principal stresses are vertical/horizontal.

6.3 Stimulation System Design

The stimulation and flow system for Experiment 2 was designed to be robust, reliable, remote-controlled, and modular. With those guiding principles and a few design constraints including the small alcove footprint, flow rates of ~13 Lpm, and pressures of up to ~ 50 MPa, a few fundamental design decisions were made. To minimize head losses while maintaining relatively small plumbing components, an orifice diameter of ~12mm was selected. These constraints led to selection of plumbing standards, as well as the plumbing design which was kept to be as 2 dimensional as possible to minimize its footprint in the alcove. The modularity of the system was needed because there are 5 boreholes which could be used for injection or production. This means that each of the borehole injection/production lines has identical plumbing, lines, and packer. This provides for robust design in that there are a minimal number of spare parts required for the system, and should one panel fail, one of the others could be used to replace it until parts are available. An example of the modular plumbing is shown in Figure 16. Figure 17 shows the system installed on the 4100 level.

The system can be operated remotely from anywhere with internet access. Although many will be able to view the data live on another system, control of the system is limited to a specific list of individuals who can remotely access the control computer from outside the mine and change pressures/flows/valving. This allows for multiple people to have access and monitor the system 24/7 and if needed change flow parameters. This includes the ability to run the supply fluid through a reverse osmosis system to reduce the conductivity of the injected water to inject a "tracer" at any time, or change the temperature of the injected water. The control system is built with a custom LabVIEW VI, and control is implemented with National Instruments hardware.

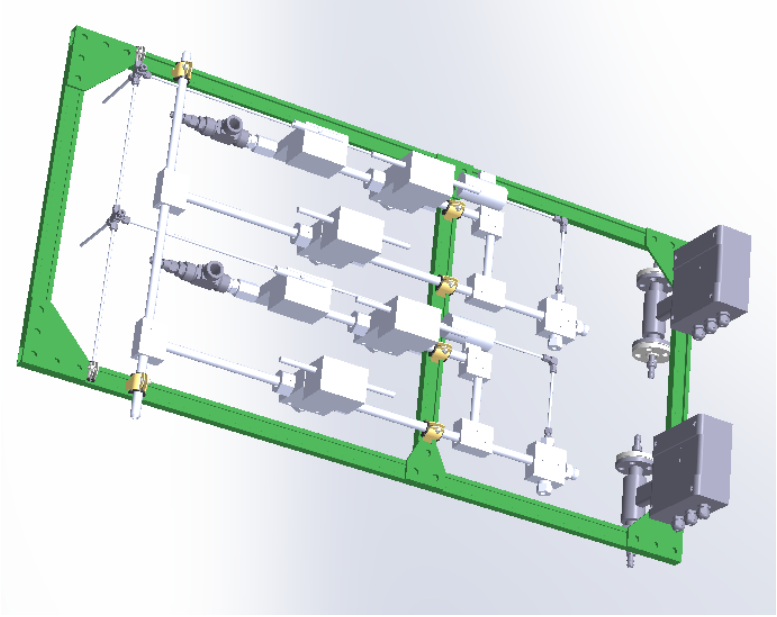

Figure 16: CAD model of the modular plumbing for one of the packer systems.

Figure 17: Panoramic of the system as installed on the 4100 level. Note the modular plumbing hung on the wall behind the other equipment and the control computer.

7 CONCLUDING REMARKS

The EGS Collab project Experiment 1 is complete, and data and papers are readily available. The Experiment 2 testbed is nearly complete, and is in a stress, rock type, and fractured environment that is quite different from Experiment 1. The Experiment 2 design considers the complex geology including stress and fracture set orientations, types of fractures and whether they are healed, and the presence of a lower-stress rhyolite layer. Spatial constraints from working in a smaller drift and the drift orientation were also addressed in addition to lessons learned from Experiment 1 including spacing the monitoring wells more, and customizing the grout for monitoring wells. The new testbed contains an injection well surrounded by four production wells, all of which will be used for monitoring flows and pressures. These wells are well-placed within the densely instrumented test bed, and oriented to intersect fractures most likely to shear. The geophysical monitoring tools are optimized for the testbed and the experiment, and are expected to provide excellent high-resolution data to allow observing and quantifying processes that occur during the experiment. Tools explicitly designed to measure shear will be used in the stimulation well, and also at a distance from the stimulation location. The very well optimized mechanical system built for this experiment addresses concerns identified in Experiment 1 and also can almost entirely be operated remotely once packers are placed.

We expect many challenges. The healed nature of most fractures is expected to present challenges, as is the shear-to-normal stress ratio. We have a number of strategies we are considering depending on observations, and are eager to begin stimulating the testbed.

ACKNOWLEDGMENTS

This material was based upon work supported by the U.S. Department of Energy, Office of Energy Efficiency and Renewable Energy

(EERE), Office of Technology Development, Geothermal Technologies Office, under Award Number DE-AC02-05CH11231 with LBNL and other awards to other national laboratories. The United States Government retains, and the publisher, by accepting the article for publication, acknowledges that the United States Government retains a non-exclusive, paid-up, irrevocable, world-wide license to publish or reproduce the published form of this manuscript, or allow others to do so, for United States Government purposes. The research supporting this work took place in whole or in part at the Sanford Underground Research Facility in Lead, South Dakota. The assistance of the Sanford Underground Research Facility and its personnel in providing physical access and general logistical and technical support is gratefully acknowledged. We also thank the crew from RESPEC, who logged the core upon recovery from drilling, and also supported the wireline logging operations. The earth model output for this paper was generated using Leapfrog Software, copyright Seequent Limited. Leapfrog and all other Seequent Limited product or service names are registered trademarks or trademarks of Seequent Limited.

REFERENCES

Ajo-Franklin, J. B., M. Schoenball, T. Wood, M. Robertson, P. Petrov, L. Huang, . . . EGS Collab Team (2018), Imaging Hydraulic Fracture Propagation Using Semi-Permanent Continuous Active Seismic Source Monitoring: Results from the DOE EGS Collab Experiment, paper presented at American Geophysical Union Fall Meeting 2018, American Geophysical Union, Washington DC, December 12, 2018.

Augustine, C. (2016), Update to Enhanced Geothermal System Resource Potential Estimate, *GRC Transactions*, *40*, 6.

Burghardt, J., T. Doe, M. Ingraham, P. Schwering, C. Ulrich, W. M. Roggenthen, . . . EGS Collab Team (2020), Integration of Shut-In Pressure Decline, Flow back, Hydraulic and Sleeve Re-Opening Tests to Infer In-Situ Stress, paper presented at 54th U.S. Rock Mechanics/Geomechanics Symposium.

Caddey, S. W., R. L. Bachman, T. J. Campbell, R. R. Reid, and R. P. Otto (1991), The Homestake gold mine, an early Proterozoic iron-formation-hosted gold deposit, Lawrence County, South Dakota, *1857J*.

Chai, C., M. Maceira, H. J. Santos-Villalobos, S. V. Venkatakrishnan, M. Schoenball, and EGS Collab Team (2020), Automatic Seismic Phase Picking Using Deep Learning for the EGS Collab project, paper presented at 45th Workshop on Geothermal Reservoir Engineering, Stanford University, Stanford, California, February 10-12, 2020.

Chi, B., L. Huang, K. Gao, J. Ajo-Franklin, T. J. Kneafsey, J. Hampton, and EGS Collab Team (2020), Anisotropic Imaging of Created Fractures in EGS Collab Experiments Using CASSM Data, paper presented at 45th Workshop on Geothermal Reservoir Engineering, Stanford University, Stanford, California, February 10-12, 2020.

Dobson, P., T. Kneafsey, J. Morris, A. Singh, M. Zoback, W. Roggenthen, . . . EGS Collab Team (2018), The EGS Collab Hydroshear Experiment at the Sanford Underground Research Facility – Siting Criteria and Evaluation of Candidate Sites, paper presented at Geothermal Resources Council 2018 Annual Meeting, Geothermal Resources Council Transactions, Reno, NV.

Dobson, P., T. J. Kneafsey, D. Blankenship, J. Morris, P. Fu, H. Knox, . . . EGS Collab Team (2021), The EGS Collab Project – Fracture Stimulation and Flow Experiments for Coupled Process Model Validation at the Sanford Underground Research Facility (SURF), South Dakota, USA, paper presented at World Geothermal Congress 2020+1 Reykjavik, Iceland, April - October 2021.

Fu, P., M. Schoenball, J. B. Ajo-Franklin, C. Chai, M. Maceira, J. P. Morris, . . . EGS Collab Team (2021a), Close Observation of Hydraulic Fracturing at EGS Collab Experiment 1: Fracture Trajectory, Microseismic Interpretations, and the Role of Natural Fractures, *Journal of Geophysical Research: Solid Earth*, *126*(7), e2020JB020840, doi:https://doi.org/10.1029/2020JB020840.

Fu, P., M. Schoenball, J. Morris, J. Ajo-Franklin, H. Knox, T. Kneafsey, . . . EGS Collab Team (2019), Microseismic Signatures of Hydraulic Fracturing: A Preliminary Interpretation of Intermediate-Scale Data from the EGS Collab Experiment, paper presented at 44th Workshop on Geothermal Reservoir Engineering, Stanford University, Stanford, California, February 11-13, 2019.

Fu, P., H. Wu, J. P. Morris, P. C. Schwering, C. Ulrich, and EGS Collab Team (2021b), Simulating Hydraulic Fracture Stimulations at the EGS Collab: Model Validation from Experiments 1 and Design-Phase Simulation for Experiment 2, paper presented at 46rd Workshop on Geothermal Reservoir Engineering, Stanford University, Stanford, California.

Guglielmi, Y., F. Cappa, J.-P. Avouac, P. Henry, and D. Elsworth (2015), Seismicity triggered by fluid injection–induced aseismic slip, *Science*, *348*(6240), 1224.

Guglielmi, Y., P. Cook, F. Soom, P. Dobson, T. Kneafsey, B. Valley, . . . F. Basirat (2021a), Estimating Stress from Three-Dimensional Borehole Displacements Induced by Fluid Injection in Different Types of Fractured or Faulted Rocks, paper presented at 55th US Rock Mechanics/Geomechanics Symposium, Houston, Texas, USA, 20-23 June 2021.

Guglielmi, Y., P. Cook, F. Soom, M. Schoenball, P. Dobson, and T. Kneafsey (2021b), In Situ Continuous Monitoring of Borehole Displacements Induced by Stimulated Hydrofracture Growth, *Geophysical Research Letters*, *48*, e2020GL090782, doi:https://doi.org/10.1029/2020GL090782.

Guglielmi, Y. G., F. Cappa, J. Rutqvist, C. F. Tsang, J. Wang, H. Lançon, . . . J. B. Janowczyk (2014), Step-Rate Injection Method for Fracture In-Situ Properties (SIMFIP): Monitoring Fractures Stimulation Efficiency, paper presented at 48th U.S. Rock Mechanics/Geomechanics Symposium, American Rock Mechanics Association, Minneapolis, Minnesota, 2014/8/18/.

Heise, J. (2015), The Sanford Underground Research Facility at Homestake, *Journal of Physics: Conference Series*, *606*(1), 26.

Ingraham, M. D., P. C. Schwering, J. Burghardt, C. Ulrich, T. Doe, W. M. Roggenthen, and C. Reimers (2020), Analysis of Hydraulic Fracturing on the 4100 Level at the Sanford Underground Research Facility, paper presented at 54th U.S. Rock Mechanics/Geomechanics Symposium, American Rock Mechanics Association, 2020/9/18.

Johnson, T., C. Strickland, H. Knox, J. Thomle, V. Vermuel, C. Ulrich, . . . EGS Collab Team (2019), EGS Collab Project Electrical Resistivity Tomography Characterization and Monitoring Status, paper presented at 44th Workshop on Geothermal Reservoir Engineering, Stanford University, Stanford, California, February 11-13, 2019.

Johnson, T. C., J. Burghardt, C. Strickland, H. Knox, V. Vermeul, M. White, . . . EGS Collab Team (2021), 4D Proxy Imaging of Fracture Dilation and Stress Shadowing Using Electrical Resistivity Tomography During High Pressure Injections Into a Dense Rock Formation, *Journal of Geophysical Research: Solid Earth*, *126*(11), e2021JB022298, doi:https://doi.org/10.1029/2021JB022298.

Kneafsey, T., D. Blankenship, P. Dobson, M. White, J. P. Morris, P. Fu, . . . EGS Collab Team (2021), Fracture Stimulation and Chilled-water Circulation Through Deep Crystalline Rock: Characterization, Modeling, Monitoring, and Heat-transfer Assessment, paper presented at 46th Workshop on Geothermal Reservoir Engineering, Stanford University, Stanford, California, February 15-17, 2021.

Kneafsey, T. J., D. Blankenship, P. F. Dobson, J. P. Morris, M. D. White, P. Fu, . . . EGS Collab Team (2020), The EGS Collab Project: Learnings from Experiment 1, paper presented at 45th Workshop on Geothermal Reservoir Engineering, Stanford University, Stanford, California, February 10-12, 2020.

Lisenbee, A. L., and M. Terry (2009), Development of a 3-D structural geology model of Homestake's 4100 to 5000 levels at the proposed location of the large cavities, *SDSMT Contract #09-05*, 33 pp.

Mattson, E., G. Neupane, A. Hawkins, J. Burghardt, M. Ingraham, M. Plummer, and EGS Collab Team (2019a), Fracture Tracer Injection Response to Pressure Perturbations at an Injection Well, *GRC Transactions*, *43*.

Mattson, E., Y. Zhang, A. Hawkins, T. Johnson, J. Ajo-Franklin, G. Neupane, and EGS Collab Team (2019b), Preliminary Collab Fracture Characterization Results from Flow and Tracer Testing Efforts paper presented at 44th Workshop on Geothermal Reservoir Engineering, Stanford University, Stanford, California, February 11-13, 2019.

Meng, M., L. P. Frash, W. Li, N. J. Welch, and J. W. Carey (2021a), Measurement of Geomechanical and Hydrological Properties of EGS-Collab Geothermal Rocks, paper presented at 55th US Rock Mechanics/Geomechanics Symposium, Houston, Texas, USA, 20-23 June 2021.

Meng, M., L. P. Frash, W. Li, N. J. Welch, J. W. Carey, C. Ulrich, and T. J. Kneafsey (2021b), Hydro-mechanical measurements of sheared crystalline rock fractures with applications for EGS Collab experiments 1 & 2, *Journal of Geophysical Research - Solid Earth*, *accepted*.

Morris, J. P. (2021), Fat Crayon Toolkit, https://www.osti.gov/biblio/1764513.

Morris, J. P., P. Fu, P. Dobson, J. Ajo-Franklin, T. J. Kneafsey, H. Knox, . . . EGS Collab Team (2018), Experimental Design for Hydrofracturing and Fluid Flow at the DOE EGS Collab Testbed.

Neupane, G., E. D. Mattson, M. A. Plummer, and EGS Collab Team (2020), Results of Multiple Tracer Injections into Fractures in the EGS Collab Testbed-1, paper presented at 45th Workshop on Geothermal Reservoir Engineering, Stanford University, Stanford, California, February 10-12, 2020.

Oldenburg, C. M., P. F. Dobson, Y. Wu, P. J. Cook, T. J. Kneafsey, S. Nakagawa, . . . J. Heise (2017), Hydraulic fracturing experiments at 1500 m depth in a deep mine: Highlights from the kISMET project, paper presented at 42nd Workshop on Geothermal Reservoir Engineering, Stanford University.

Pan, W., L. Huang, K. Gao, J. Ajo-Franklin, T. J. Kneafsey, and EGS Collab Team (2019), Anisotropic Full-Waveform Inversion and Least-Squares Reverse-Time Migration of CASSM Data for Experiment I of the EGS Collab Project paper presented at 44th Workshop on Geothermal Reservoir Engineering, Stanford University, Stanford, California, February 11-13, 2019.

Schoenball, M., J. Ajo-Franklin, D. Blankenship, P. Cook, P. Dobson, Y. Guglielmi, . . . EGS Collab Team (2019), Microseismic monitoring of meso-scale stimulations for the DOE EGS Collab project at the Sanford Underground Research Facility, paper presented at 44th Workshop on Geothermal Reservoir Engineering, Stanford University, Stanford, California, February 11-13, 2019.

Schoenball, M., J. B. Ajo-Franklin, D. Blankenship, C. Chai, A. Chakravarty, P. Dobson, . . . EGS Collab Team (2020a), Creation of a Mixed-Mode Fracture Network at Mesoscale Through Hydraulic Fracturing and Shear Stimulation, *Journal of Geophysical Research: Solid Earth*, *125*(12), e2020JB019807, doi:https://doi.org/10.1029/2020JB019807.

Schoenball, M., J. B. Ajo-Franklin, T. Wood, M. Robertson, P. Cook, V. Rodriguez-Tribaldos, . . . EGS Collab Team (2020b), Lessons learned from passive seismic monitoring of EGS Collab Experiment 1, paper presented at 45th Workshop on Geothermal Reservoir Engineering, Stanford University, Stanford, California, February 10-12, 2020.

Schoenball, M., Y. Guglielmi, J. B. Ajo-Franklin, P. J. Cook, P. Dobson, C. Hopp, . . . C. Ulrich (2021), In-situ observation of pre-, co- and post-seismic shear slip at 1.5 km depth, *Earth and Space Science Open Archive* doi:10.1002/essoar.10506700.1.

Singh, A., M. Zoback, P. F. Dobson, T. J. Kneafsey, M. Schoenball, Y. Guglielmi, . . . EGS Collab Team (2019), Slip tendency analysis of fracture networks to determine suitability of candidate testbeds for the EGS Collab hydroshear experiment, *Geothermal Resources Council Transactions*, *43*, 405–424.

Stetler, L. D. (2015), Water geochemistry and pressure buildup in drill holes on the 4950-ft level at the Sanford Underground Research Facility, paper presented at Proceedings of the South Dakota Academy of Sciences.

Templeton, D., J. Morris, M. Schoenball, T. Wood, M. Robertson, P. Cook, . . . EGS Collab Team (2019), Microseismic Correlation and Cluster Analysis of DOE EGS Collab Data, paper presented at 44th Workshop on Geothermal Reservoir Engineering, Stanford University, Stanford, California, February 11-13, 2019.

Ulrich, C., P. F. Dobson, T. J. Kneafsey, W. M. Roggenthen, N. Uzunlar, T. W. Doe, . . . EGS Collab Team (2018), The Distribution, Orientation, and Characteristics of Natural Fractures for Experiment 1 of the EGS Collab Project, Sanford Underground Research Facility, paper presented at 52nd U.S. Rock Mechanics/Geomechanics Symposium, American Rock Mechanics Association, Seattle, Washington, 2018/8/21.

Wang, H. F., M. Y. Lee, T. W. Doe, B. C. Haimson, C. M. Oldenburg, and P. F. Dobson (2017), In-Situ Stress Measurement at 1550-Meters Depth at the kISMET Test Site in Lead, S.D, paper presented at 51st U.S. Rock Mechanics/Geomechanics Symposium, American Rock Mechanics Association, San Francisco, California, USA, 2017/8/28/.

White, M., T. Johnson, T. Kneafsey, D. Blankenship, P. Fu, H. Wu, . . . EGS Collab Team (2019), The Necessity for Iteration in the Application of Numerical Simulation to EGS: Examples from the EGS Collab Test Bed 1, paper presented at 44th Workshop on Geothermal Reservoir Engineering, Stanford University, Stanford, California, February 11-13, 2019.

White, M. D., J. A. Burghardt, and EGS Collab Team (2021), Modeling the Dynamic Flow Resistance Across the Fracture Network of EGS Collab Experiment 1, paper presented at 46th Workshop on Geothermal Reservoir Engineering, Stanford University, Stanford, California, February 15-17, 2021.

White, M. D., P. Fu, and EGS Collab Team (2020), Application of an Embedded Fracture and Borehole Modeling Approach to the Understanding of EGS Collab Experiment 1, paper presented at 45th Workshop on Geothermal Reservoir Engineering, Stanford University, Stanford, California, February 10-12, 2020.

White, M. D., P. Fu, A. Ghassemi, H. Huang, J. Rutqvist, B. Johnston, and EGS Collab Team (2018), Numerical Simulation Applications in the Design of EGS Collab Experiment 1, paper presented at 43rd Workshop on Geothermal Reservoir Engineering, Stanford University, Stanford, California, February 12-14, 2018.

Williams, C. F., M. J. Reed, R. H. Mariner, J. DeAngelo, and S. P. Galanis, Jr. (2008), Assessment of moderate- and high-temperature geothermal resources of the United States, Type United States Geological Survey Fact Sheet 2008-3082, 4 pp.

Wu, H., P. Fu, J. P. Morris, R. R. Settgast, F. J. Ryerson, E. D. Mattson, . . . Y. Zhang (2019), Stochastic modeling of a conservative tracer test for the characterization of fracture flow patterns in EGS Collab Experiment 1, paper presented at 53rd US Rock Mechanics/Geomechanics Symposium, American Rock Mechanics Association, New York, NY, USA, 23–26 June 2019.